Acta Pharmaceutica Sinica B 2024;14(9):3916−3930

Chinese Pharmaceutical Association
Institute of Materia Medica, Chinese Academy of Medical Sciences

Acta Pharmaceutica Sinica B

www.elsevier.com/locate/apsb
www.sciencedirect.com

ORIGINAL ARTICLE

Icaritin inhibits the progression of urothelial cancer by suppressing PADI2-mediated neutrophil infiltration and neutrophil extracellular trap formation

Zezhong Mou [a,b,†], Yiling Chen [a,b,†], Jinzhong Hu [a,b,†], Yun Hu [a,b,†], Lujia Zou [a,b], Xinan Chen [a,b], Shenghua Liu [a,b], Qiuping Yin [a], Jian Gong [a], Shuchen Li [a], Shanhua Mao [a,b,*], Chenyang Xu [a,b,*], Haowen Jiang [a,b,c,*]

[a]*Department of Urology, Huashan Hospital, Fudan University, Shanghai 200040, China*
[b]*Fudan Institute of Urology, Fudan University, Shanghai 200040, China*
[c]*National Clinical Research Center for Aging and Medicine, Fudan University, Shanghai 200040, China*

Received 28 February 2024; received in revised form 5 May 2024; accepted 17 June 2024

KEY WORDS

Icaritin;
Neutrophil;
Neutrophil extracellular trap;
PADI2;
Urothelial cancer

Abstract Tumor relapse and metastasis are the major causes of mortality associated with urothelial cancer. In the tumor microenvironment, negative regulatory molecules and various immune cell subtypes suppress antitumor immunity. The inflammatory microenvironment, associated with neutrophils and neutrophil extracellular traps (NETs), promotes tumor metastasis. However, no drugs are currently available to specifically inhibit neutrophils and NETs. In this study, we first demonstrated that icaritin (ICT), a Chinese herbal remedy that is a first-line treatment for advanced and incurable hepatocellular carcinoma, reduces NETs caused by suicidal NETosis and prevents neutrophil infiltration in the tumor microenvironment. Mechanistically, ICT binds to and inhibits the expression of PADI2 in neutrophils, thereby suppressing PADI2-mediated histone citrullination. Moreover, ICT inhibits ROS generation, suppresses the MAPK signaling pathway, and inhibits NET-induced tumor metastasis. Simultaneously, ICT inhibits tumoral PADI2-mediated histone citrullination, which consequently suppresses the transcription of neutrophil-recruiting genes such as GM-CSF and IL-6. The downregulation of IL-6 expression, in turn, forms a regulatory feedback loop through the JAK2/STAT3/IL-6 axis. Through a retrospective study of

*Corresponding authors.
E-mail addresses: maoshanhua@163.com (Shanhua Mao), doctoralex7@163.com (Chenyang Xu), urology_hs@163.com (Haowen Jiang).
[†]These authors made equal contributions to this work.

Peer review under the responsibility of Chinese Pharmaceutical Association and Institute of Materia Medica, Chinese Academy of Medical Sciences.

https://doi.org/10.1016/j.apsb.2024.06.029

clinical samples, we found a correlation between neutrophils, NETs, UCa prognosis, and immune evasion. Combining ICT with immune checkpoint inhibitors may have synergistic effects. In summary, our study demonstrated that ICT could be a novel inhibitor of NETs and a novel UCa treatment.

1. Introduction

Urothelial cancer ranks among the most common urologic cancers. Tumor recurrence and metastasis serve as major prognostic factors[1]. In 2023, an estimated 168,560 urologic cancer cases were diagnosed in the United States, with approximately 32,590 fatalities; urothelial cancer comprises approximately 50% of these cases[2]. Moreover, in China, an estimated 244,300 cases of urologic cancer were diagnosed in 2022, accompanied by approximately 78,900 fatalities[3]. Despite the availability of new treatment options, such as platinum-based chemotherapy and PD1 antibody-based immunotherapy, more than half of urothelial cancer patients still do not respond to these treatments. Therefore, to improve the prognosis of urothelial carcinoma patients, research on novel therapeutic medicines is desperately needed.

Icariin (ICA) is the main active ingredient in Epimedium, a traditional Chinese medicine used as a tonic, aphrodisiac, and anti-rheumatic agent. Once ingested, ICA is metabolized into Icaritin (ICT), which then exerts its effects[4]. ICA exhibits various biological activities, including regulating adaptive immunity, possessing antioxidant properties, and inhibiting tumor progression[4-7]. In 2022, the Icaritin capsule, featuring ICT as its main ingredient, received approval from the China National Medical Products Administration (NMPA) for first-line treatment of advanced, inoperable hepatocellular carcinoma. Furthermore, it has demonstrated significant efficacy in prolonging the overall survival of patients with advanced hepatocellular carcinoma. ICT not only directly plays a role in killing tumors by inducing apoptosis and autophagy but also regulates the tumor immune microenvironment and promotes an antitumor immune response[8-11]. However, the specific mechanisms through which ICT regulates the TME, particularly in urothelial cancer, are not yet fully understood.

The most prevalent innate immune effector cells in the human body are neutrophils. Neutrophils not only fight pathogens but are also involved in the development of cancer, autoimmunity, and acute damage healing[12-15]. Studies have shown that neutrophils exhibit antitumor effects in early-stage tumors *via* ROS release, whereas in later stages, they may promote tumor progression[16]. Neutrophils operate through three primary pathways in the microenvironment: phagocytosis, degranulation, and neutrophil extracellular traps (NETs) release. NETs, large extracellular web-like structures composed of cytosolic and granule proteins assembled on a scaffold of decondensed chromatin, were first proposed in 2004[17]. Neutrophils are released *via* two mechanisms: suicidal NETosis and vital NETosis. NETosis, the primary mode of NET release, represents a unique form of neutrophil death. In this process, the MEK/ERK signaling pathway triggers ROS generation, activating the downstream myeloperoxidase (MPO) pathway. MPO mediates the activation of neutrophil elastase (NE), degrading the actin cytoskeleton in the cytoplasm and promoting chromatin decondensation.

Furthermore, MPO stimulates PAD family 2/4, which results in histone citrullination and further promotes chromatin decondensation[18]. Recently, the relationship between NETs and cancer has gained increasing recognition[19]. Clinical evidence indicates that elevated levels of NETs correlate with poor prognosis in patients with various tumors[17,20-24]. Studies have also shown that NETs facilitate the epithelial−mesenchymal transition (EMT) of endothelial cells[25]. Furthermore, tumor cells can also induce NET generation, thereby protecting themselves from NK- and T-cell-mediated destruction[26]. However, research on NETs in urothelial cancer is limited, and there is still a lack of stable NET inhibitors. Identifying potential targets and agents to inhibit NETs is crucial for advancing antitumor therapy.

The first evidence that ICT prevents urothelial carcinoma metastases by decreasing NETs formation and neutrophil infiltration in the tumor microenvironment was shown in this study. Using Biacore and Western blot analysis, we directly demonstrated that ICT binds to and inhibits PADI2, a protein related to histone citrullination. The regulation of PADI2 by ICT affects tumor cells and neutrophils differently: in neutrophils, it inhibits suicidal NETosis and reduces NET production by inhibiting PADI2, thereby decreasing histone citrullination. In tumor cells, ICT inhibits PADI2-induced histone citrullination, which decreases IL-6 transcription, further inhibiting the IL-6/JAK2/STAT3/IL-6 feedback loop and limiting neutrophil recruitment. Additionally, we propose that NETs could serve as a novel prognostic marker for urothelial cancer and that ICT, in combination with PD1 inhibitors, can counteract NET-induced T-cell depletion in a clinical setting.

2. Materials and methods

2.1. Cell culture

MB49 murine urothelial tumor cells were obtained from Millipore Corporation (Millipore, USA), and the Hepa 1-6 murine hepatoma cell line and the T24 and UMUC-3 human urothelial cancer cell lines were purchased from ATCC (USA). All cell lines generated in this study (T24, UMUC-3, MB49, and Hepa 1-6) were cultured in complete DMEM (GE Healthcare Life Sciences, USA) supplemented with 10% fetal bovine serum (FBS; Gibco; Thermo Fisher Science, USA) and 100 mg/mL penicillin/streptomycin (Yeason Biotechnology, China) at 37 °C in a 5% CO_2 humidified incubator. Luciferase-expressing (MB49-luc) cells were generated as previously described[27]. Cell cultures at passages 5−8 were used and tested for mycoplasma contamination every month.

2.2. Cell viability assay

The effect of icaritin (ICT) (Winherb, China) on tumor cell viability was evaluated using the CCK-8 Cell Counting Kit (Life-

iLab, China). The cell viability for each treatment was determined as % cell inhibition, which was calculated by Eq. (1):

$$\text{Cell inhibition (\%)} = [(A_{450\ \text{sample}} - A_{450\ \text{background}})/(A_{450\ \text{control}} - A_{450\ \text{background}})] \times 100 \quad (1)$$

2.3. Cell migration and invasion assays

Migration and invasion assays were conducted using wound healing and Transwell methods. For the wound healing assay, 5×10^5 cells were seeded in 6-well plates. A micropipette tip was used to gently scratch the center of each well, followed by a 48-h treatment with ICT.

Cell migration images were captured at 0 and 48 h. In the Transwell assay, 1×10^4 cells in 200 μL of serum-free DMEM were placed in the upper chamber of Matrigel-coated Transwell inserts (Corning, USA), and 400 μL of complete DMEM was added to the lower chambers. After 24 h of ICT treatment, the cells were collected, fixed, stained with 0.5% crystal violet, and then photographed using an inverted microscope (Olympus, Germany).

2.4. Murine model and study design

All animal studies were approved by the Ethics Committee and performed in accordance with ethical standards. Male wild-type C57BL/6J mice (Phenotek, China) between 6 and 8 weeks of age were used and maintained in specific pathogen-free conditions in animal facilities (Fudan University, China). A tumor-bearing murine model was constructed by subcutaneous injection of the murine urothelial cancer carcinoma cell line MB49 (3×10^5 cells) and murine hepatoma cell line Hepa 1-6 (3×10^5 cells). For the orthotopic urothelial cancer model, male wild-type C57BL/6J mice were anesthetized *via* injection of 1.5% tribromoethanol (AIBI Bio-Technology, China). A minor incision was made in the lower abdomen to reveal the bladder, into which MB49 or MB49-luc (3×10^5 cells) cells were injected using a 28-gauge needle.

Icaritin was dissolved in corn oil, and the mice were gavaged two times per day. PMA (Sigma−Aldrich, USA) was intratracheally administered to mice by dissolving it at a dose of 200 μg/kg in 40 μL of sterile saline. DNase I treatment involved i.p. injection of 5 mg/kg DNase I (Sigma−Aldrich, USA) 1 day before tumor cell injection, followed by daily injection of the reagents for 7 days and then twice a week. Neutrophil *in vivo* depletion was performed using 200 μg of anti-Ly6G (BioXcell, USA) per mouse. The size and volume of the tumors were observed, and growth curves were plotted. The experimental endpoint was defined as death or a tumor volume $\geq$2000 mm^3. Tumor volume was calculated using Eq. (2):

$$\text{Tumor volume} = \text{Length} \times \text{Width} \times \text{Width}/2 \quad (2)$$

2.5. Clinical sample collection and processing

All tumor tissue samples collected between 2015 and 2021 were pathologically diagnosed with urothelial carcinoma. Patients lacking pathological, clinical, or survival information were excluded. A total of 195 paraffin-embedded UCa samples, 24 fresh Uca samples, and 40 blood serum samples were obtained from patients undergoing surgery at Huashan Hospital (Fudan University, China). Tissue detachment from TMAs and IHC staining analysis followed previously described methods[27]. Each sample was confirmed pathologically by two pathologists. The Institutional Ethical Review Board for Research on Human Subjects at Huashan Hospital approved the use of these tissue samples and associated clinicopathological information.

2.6. Immunohistochemical staining

For immunohistochemistry (IHC) staining, dewaxed tissue sections were processed. The sections were rehydrated and heated in a 10 mmol/L citrate solution (pH 6.0) for antigen retrieval, followed by treatment with 3% H_2O_2/MeOH to suppress endogenous peroxidase activity. The sections were treated with a 10% horse serum-blocking solution to prevent nonspecific binding. Primary antibodies were applied to the sections, which were then incubated at 4 °C for 16 h in a humidified chamber. Subsequently, the sections were treated with a biotin-conjugated goat anti-mouse/rabbit IgG secondary antibody. The sections were washed three times with PBS to remove unbound antibodies. Visualization was achieved with a DAB substrate kit. Finally, the slides were digitally scanned with the Pannoramic SCAN II system. Antibody information is listed in Supporting Information Table S1.

2.7. Cell isolation and flow cytometry analysis

Flow cytometry was employed for subpopulation and functional analyses of neutrophils and lymphocytes in both murine and fresh human tumor tissues. Mice were anesthetized and euthanized at specific predetermined time points. Murine and fresh human tumor tissues were isolated and incubated with RPMI-1640, 5% FBS, collagenase IA (1 mg/mL, Sigma−Aldrich), and DNase I (1 mg/mL, Sigma−Aldrich) at 37 °C for 45 min. Subsequently, the digested tissues were filtered through 70 μm cell strainers, and the cells were centrifuged at 300×*g* for 10 min. After resuspension, the red blood cells were lysed with red blood cell lysis buffer (Yeason Biotechnology, China). Details of the antibodies used for flow cytometric analysis can be found in Table S1. The data were analyzed with FlowJo software (version 10.8.1, FlowJo, LLC).

2.8. Neutrophil isolation

Neutrophils were isolated from the peripheral blood of healthy donors or mouse bone marrow by using a neutrophil separation kit (Solarbio, China), murine neutrophil separation beads (TBD, China) and bone marrow neutrophil separation kit (Solarbio, China). The purity of the isolated neutrophils was determined by flow cytometry.

2.9. Neutrophil migration assays

UMUC-3 urothelial cancer cells were seeded in the lower chambers and cultured under various conditions for 24 h. Freshly isolated neutrophils suspended in RPMI-1640 (Gibco; Thermo Fisher Science, USA) were subsequently added to the upper chambers. After 12 h of coculture, neutrophils that migrated to the lower chambers were quantified by flow cytometry, while those in the upper chambers were stained and quantified using 0.5% Crystal Violet Stain Solution (Yeason Biotechnology, China).

2.10. NET generation

The freshly isolated neutrophils were incubated with 500 nmol/L PMA for 4 h at 37 °C in a 5% CO_2 environment. Then, the media was discarded, the cells were washed, and the NETs adhering to the bottom were collected with cold PBS. The NETs were collected by centrifugation for 10 min at 18,000×*g* and 4 °C. The DNA concentration in the collected sample was measured using spectrophotometry.

2.11. Reverse transcription and quantitative real-time PCR (RT-qPCR)

Total RNA was extracted from tumor cells using the UNIQ-10 Column TRIzol Total RNA Isolation Kit (Sangon Biotech, China) according to the manufacturer's instructions. Reverse transcription was carried out using MightyScript Plus First Strand cDNA Synthesis Master Mix (gDNA digester) to synthesize cDNA (Sangon Biotech, China). RT−qPCR was conducted using Hieff UNICONR Universal Blue qPCR SYBR Green Master Mix (Yeason Biotechnology, China) on an ABI 7900HT sequence detection system (Thermo Fisher Scientific, USA). TUBB RNA served as the internal control. The $2^{-\Delta\Delta CT}$ method was used to calculate the differential expression of RNAs. These experiments were replicated three times. All the primers utilized are listed in Supporting Information Table S2.

2.12. Western blotting

The immunoblotting technique was conducted as previously described[28]. Briefly, total protein was extracted using RIPA lysis buffer (Sangon Biotech, China) supplemented with a protease and phosphatase inhibitor complex (Sangon Biotech, China). Equal quantities of cellular protein and EZ marker (Life-iLab, China) were separated using SDS-PAGE on 8%−15% gels. Immunoblots were visualized with an enhanced chemiluminescence (ECL) kit (Thermo Fisher Scientific, USA). The Western blotting results were quantified with ImageJ software. Antibody information is listed in Table S1.

2.13. Apoptosis and cell cycle analysis

Apoptosis and cell cycle analyses were performed using flow cytometry. Briefly, urothelial cancer cells were treated with or without ICT for 24 h, followed by digestion with trypsin without EDTA (Yeason Biotechnology, China) and washing with PBS. The cells were stained with Annexin V-FITC and PI using an Annexin V-FITC/PI Apoptosis Detection Kit (Yeason Biotechnology, China) to measure the percentage of apoptotic cells on a flow cytometer. For cell cycle analysis, tumor cells were stained using a cell cycle detection kit (Yeason Biotechnology, China).

2.14. Enzyme-linked immunosorbent assay (ELISA)

The levels of IL-6 in the cell culture medium were detected by using an IL-6 Human ELISA Kit (Thermo Fisher, USA), and MPO-DNA in the serum of urothelial cancer patients was detected by using an MPO-DNA ELISA Kit (Zhili Biotechnology, China) following the manufacturer's instructions.

2.15. ROS analysis

Freshly isolated neutrophils were treated with ICT and Rosup (positive control) at 37 °C in a 5% CO_2 environment to measure ROS levels. The cells were then harvested and analyzed using a Reactive Oxygen Species Assay Kit (Biosharp, China). After the cells were incubated for 15 min at 37 °C in the dark, they were washed with cold PBS and analyzed by flow cytometry or fluorescence microscopy within 30 min.

2.16. 3D spheroid culture

T24 cells were cultured on ultralow attachment surface 6-well plates (Corning, USA). 3D spheroid culture medium, a 1:1 mixture of DMEM and medium from neutrophils pretreated with or without ICT and PMA, was added to each well. The medium was changed every two to three days. Between Days 1 and 5, the number of spheroids was analyzed.

2.17. Statistical analysis

Statistical analysis was performed using GraphPad Prism (version 10.1.0, GraphPad, Bethesda, MD) and R project (version 4.3.2, R Core Team, Vienna, Austria), with the statistical significance set at $P < 0.05$. For the comparison of continuous variables, Student's *t*-tests (two-tailed) or Wilcoxon rank-sum tests were used based on the normality of the data; for categorical variables, χ^2 tests, χ^2 tests with Yates's correction, or Fisher's exact *t*-tests were chosen as appropriate. Specifically, tumor T stage was considered an ordinal categorical variable and was analyzed using ordinal multinomial logistic regression. Survival data were analyzed and compared using the Kaplan−Meier method. Correlation analysis was performed using the nonparametric Spearman correlation test. The H-score for immunohistochemical staining was automatically calculated by the Densito Quant Module in the Quant Center 2.3 analysis software as Eq. (3):

$$\begin{aligned}\text{H-SCORE} = {} & (\text{percentage of weak intensity cells} \times 1) \\ & + (\text{percentage of moderate intensity cells} \times 2) \\ & + (\text{percentage of strong intensity cells} \times 3) \end{aligned} \quad (3)$$

The cutoff values for immunohistochemical expression were wet by the median of the relative H-scores of different molecules. Specifically, the cutoff H-scores for H3CIT, CD66b, CD4, CD8, PD1, and PADI2 were 204.91, 1.90, 2.77, 1.69, 73.96, and 102.09, respectively.

3. Results

3.1. ICT inhibits the malignant biological behaviors of urothelial cancer cells in vitro

To clarify the regulatory mechanisms of ICT on tumors, its inhibitory effects on malignant biological characteristics were first assessed through *in vitro* experiments. ICT is a derivative of the pentacyclic flavonoid derived from Epimedium (Fig. 1A). The human urothelial cancer cell lines UMUC-3 and T24, along with the murine urothelial cancer cell line MB49, were treated with increasing concentrations of ICT. At 48 h, the IC_{50} values for ICT in UMUC-3, T24, and MB49 cells were 15.71, 19.55, and 9.32 μmol/L, respectively (Fig. 1B). CCK8 assays illustrated that

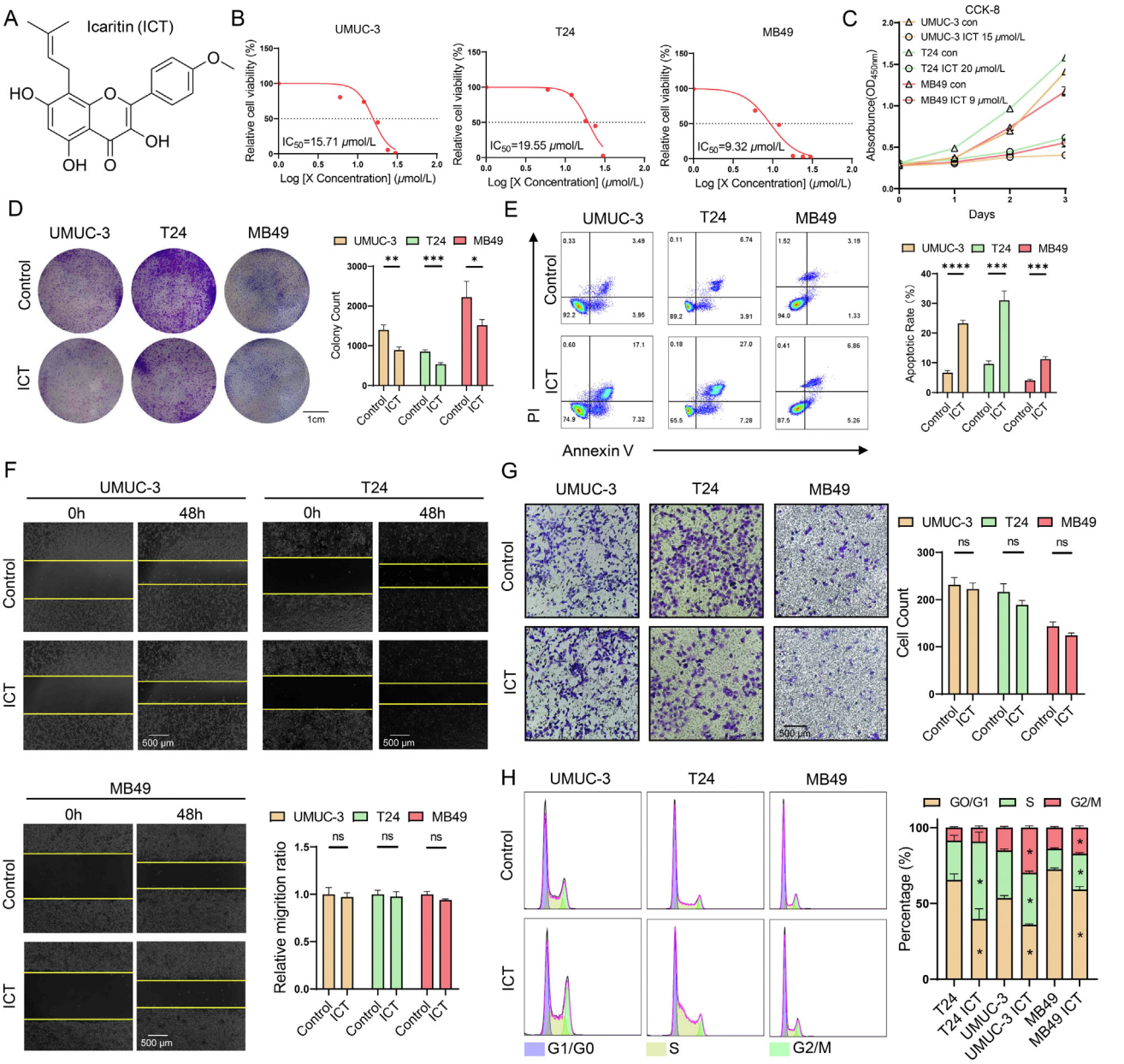

Figure 1 ICT inhibits urothelial cancer progression *in vitro*. (A) Schematic representation of the structure of ICT. (B and C) The cytotoxicity of ICT toward the human urothelial cancer cell lines UMUC-3 and T24 and the murine urothelial cancer cell line MB49 was determined by CCK-8 assays. (D) Colony formation assay of UMUC-3, T24, and MB49 cells treated with or without ICT. After staining with crystal violet, the number of colonies was quantified. All images represent data from three independent experiments. Cell viability is presented as the mean ± SD. Significance was assessed using Student's *t*-test (*$P < 0.05$, **$P < 0.01$, ***$P < 0.001$). (E) The apoptosis of UMUC-3, T24, and MB49 cells treated with or without ICT was assessed by FITC-conjugated Annexin V-FITC and PI staining. The percentages of apoptotic cells are graphed and shown as the mean ± SD. Significance was assessed using Student's *t*-test (***$P < 0.001$, ****$P < 0.0001$). (F) Wound healing assays were used to assess the migration of UMUC-3, T24, and MB49 cells treated with or without ICT. The cell migration is shown as the mean ± SD. Significance was assessed using Student's *t*-test (ns indicates no significance). (G) Transwell assays were used to evaluate the invasion of UMUC-3, T24, and MB49 cells treated with or without ICT. The cell invasion is shown as the mean ± SD. Significance was assessed using Student's *t*-test (ns indicates no significance). (H) Cell cycle analyses with flow cytometry in UMUC-3, T24, and MB49 cells treated with or without ICT. Significance was assessed using Student's *t*-test (*$P < 0.05$).

ICT significantly inhibited cancer cell viability (Fig. 1C), and colony formation assays further indicated that ICT inhibited tumor cell proliferation (Fig. 1D). To further evaluate the regulatory mechanism of ICT on tumor cell death, flow cytometry was performed to detect the apoptosis rates of tumor cells after ICT treatment, which revealed a significant promotion of tumor cell death caused by ICT (Fig. 1E). Subsequent *in vitro* assessments of tumor invasion capabilities (including scratch and Transwell assays) unexpectedly revealed that ICT had a less significant inhibitory effect on tumor invasion (Fig. 1F and G). Furthermore,

investigation of the modulation of the cell cycle revealed the differential effects of ICT on cell cycle arrest (S phase arrest in T24 cells and G2/M phase arrest in UMUC-3 and MB49 cells, Fig. 1H). These *in vitro* findings demonstrated the potential of ICT as an antitumor agent.

3.2. *ICT suppresses tumor metastasis by inhibiting neutrophil infiltration in vivo*

To further investigate the *in vivo* antitumor efficacy of ICT against urothelial cancer, we utilized a subcutaneous tumor model in C57BL/6J mice and administered ICT *via* oral gavage (Fig. 2A). A dose-dependent increase in tumor suppression was observed with increasing ICT concentrations (Fig. 2B and C). Assessment of liver function and measurement of body weight changes in mice treated with varying concentrations of ICT indicated its safety and efficacy *in vivo* (Supporting Information Fig. S1A−S1C). Considering these outcomes, a concentration of 30 mg/kg was selected for subsequent experimentation (Fig. 2D and E). To elucidate whether ICT-mediated tumor suppression occurs through modulation of the tumor immune microenvironment, a detailed analysis of the predominant antitumor immune cell subsets was conducted. ICT was found to enhance the infiltration of cytotoxic T cells and M1-type macrophages (Fig. 2F and G), while the levels of immune checkpoint molecules such as PD-1 and CTLA-4 and M2-type macrophages tended to decrease, albeit not significantly (Fig. 2H). The secretion of antitumor immune effector molecules was also promoted (Fig. 2I). We then examined the *in vivo* tumor-suppressive effects of ICT on hepatocellular carcinoma in mice. ICT inhibited the growth of subcutaneous tumors (Supporting Information Fig. S2A−S2D), enhanced the infiltration of CTLs, macrophages, and M1-type macrophages, and promoted the secretion of antitumor effector molecules such as IFN-γ and Granzyme B (Fig. S2F−S2I). Given the potential immunosuppressive role of neutrophils within the tumor microenvironment, intratumoral neutrophil regulation was also investigated, revealing a marked suppression of neutrophil infiltration by ICT (Fig. 2J, K, Fig. S2E). Additionally, we evaluated the suppressive impact of ICT on tumor growth in a murine orthotopic urothelial cancer model. K−M survival analysis and *in vivo* imaging confirmed the ability of ICT to inhibit the growth of murine orthotopic urothelial cancer (Supporting Information Fig. S3A−S3C). Flow cytometry analysis demonstrated that ICT's regulatory effects on the tumor microenvironment in this model were largely congruent with those observed in subcutaneous tumors, with its inhibitory effects on immune checkpoints proving more potent in the orthotopic setting (Fig. S3F). Intriguingly, tail vein pulmonary metastasis assays revealed that ICT significantly inhibited tumor metastasis *in vivo*, in contrast to our *in vitro* observations. This inhibitory effect on metastasis was diminished after neutrophil depletion in the murine model (Fig. 2L and M). Furthermore, the suppression of tumor metastasis persisted even after the separate depletion of $CD4^+$ or $CD8^+$ T cells (Fig. 2N). Based on the above findings, we hypothesized that ICT modulates neutrophils within the tumor immune microenvironment, thereby enhancing antitumor immunity by inhibiting neutrophil infiltration.

3.3. *ICT reverses NET-mediated tumor EMT and stemness to inhibit metastasis*

Neutrophil extracellular traps (NETs), as the product of NETosis in neutrophils, are pivotal in mediating immunosuppression within the tumor immune microenvironment. Consequently, we explored the regulatory effect of ICT on NET formation. Comparative analyses of subcutaneous tumors in mice treated with ICT revealed a significant reduction in the expression of the NET markers histone 3 citrullinated (H3CIT) and myeloperoxidase (MPO) (Fig. 3A). To further clarify the mechanism of ICT in tumor regulation mediated by NETs, an *in vitro* coculture system was established. The results indicated that phorbol 12-myristate 13-acetate (PMA)-induced NET formation enhanced tumor invasion and metastasis, while ICT effectively reversed this effect. Moreover, DNase I, a NET-degrading agent, exhibited synergistic effects with ICT (Fig. 3B). *In vivo* experiments further confirmed the inhibitory effect of ICT on NET formation (Fig. 3C). To explore the underlying mechanisms further, we examined the EMT phenotype of tumors after coculture. NETs were observed to facilitate EMT in tumor cells. While ICT alone moderately inhibited EMT, EMT was markedly enhanced when a NET-degrading agent was combined with ICT (Fig. 3D). To investigate the regulatory role of ICT in epithelial−mesenchymal transition (EMT) in orthotopic urothelial tumors and mesenchymal−epithelial transition (MET) in lung metastatic tumors, IHC detection of the EMT- and MET-related markers E-cadherin and N-cadherin was conducted on both orthotopic urothelial tumors and lung metastatic tumors. These findings indicate that ICT could suppress the expression of N-cadherin and enhance the expression of E-cadherin in orthotopic urothelial tumors, consistent with findings from cellular experiments. While ICT has been shown to decrease the quantity and dimensions of metastatic lung tumors, it has not been found to have a substantial impact on the regulation of N-cadherin expression and only slightly increases E-cadherin expression (Figs. S3D and S3E). Considering the established role of NETs in augmenting tumor stemness, we also assessed whether ICT might be involved. Western blot analysis indicated that ICT suppressed the expression of the stemness-related genes CD44, SOX2, and OCT4 (Fig. 3E). This finding was further validated by 3D spheroid-formation assays (Fig. 3F). Collectively, these results suggest that ICT not only inhibits neutrophil infiltration but also effectively suppresses NET formation, thereby inhibiting NET-mediated tumor EMT and stemness.

3.4. *ICT inhibits NET formation by targeting PADI2 and suppressing suicidal NETosis*

To investigate the mechanism underlying the suppression of NET formation by ICT, $CD45^+CD11b^+$ neutrophils were isolated, treated with ICT, and subjected to RNA-seq analysis (Fig. 4A). Functional enrichment analysis indicated that ICT modulated pathways related to NET formation and chemokine signaling (Fig. 4B). Differential gene expression analysis revealed a significant reduction in the expression of PADI2, a gene associated with histone citrullination and NET formation. Molecular docking experiments suggested that ICT could bind to PADI2 at six potential sites (Fig. 4C). Correlation analysis between PADI2 expression and neutrophil infiltration in urothelial cancer suggested that the expression of PADI2 was associated with neutrophil infiltration (Supporting Information Fig. S4A and S4B, and Fig. 4F) and could be used to identify NET-related genes (Fig. 4D). Gene set variation analysis (GSVA) revealed correlations between PADI2 expression and the expression of NET-associated genes (Fig. 4E, Fig. S4C and S4D), leading to the hypothesis that ICT-mediated regulation of NET formation might be related to PADI2, which was supported by Western blot

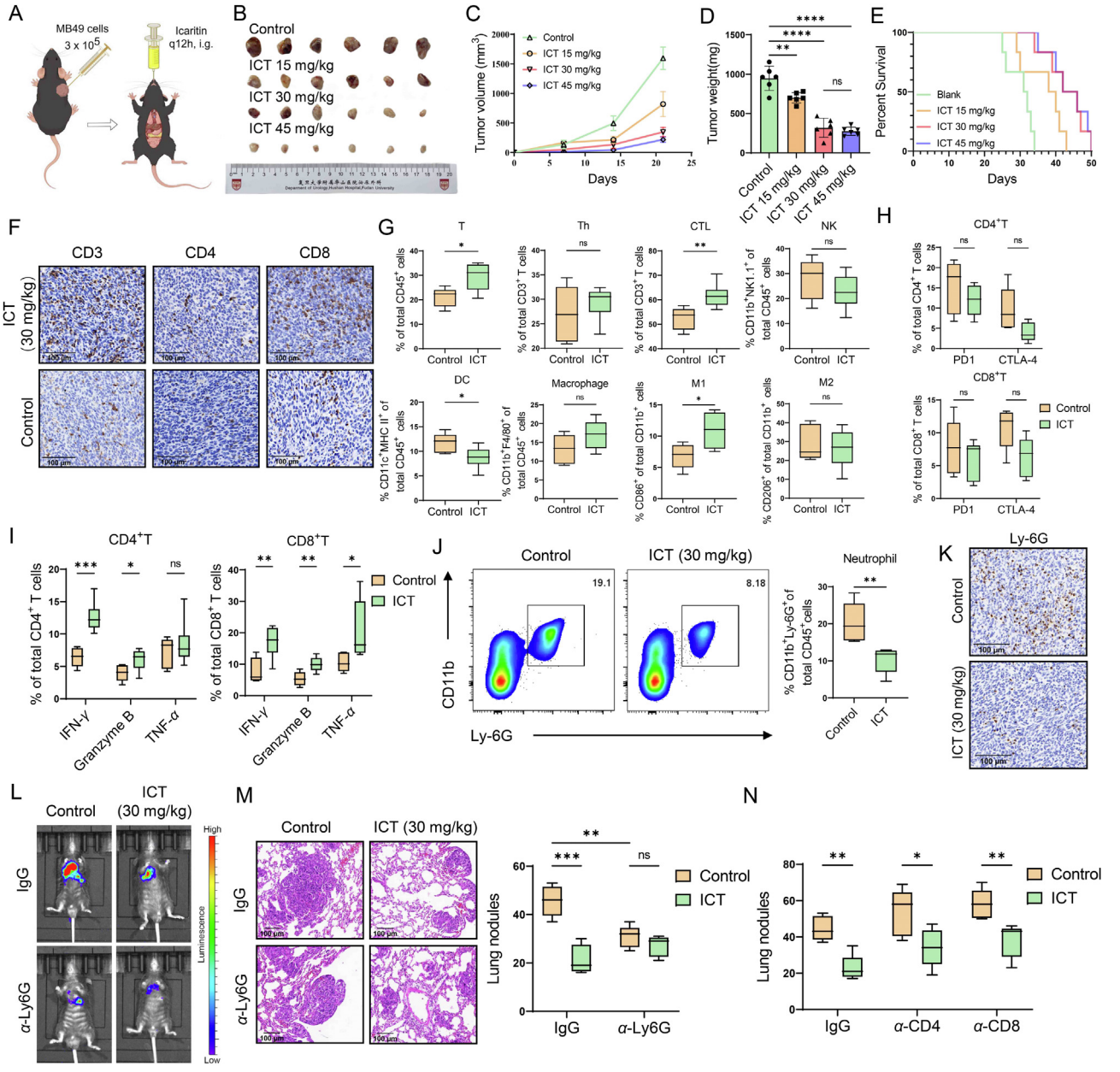

Figure 2 ICT inhibits neutrophil infiltration in the tumor microenvironment and enhances T-cell antitumor immunity. (A) Schematic diagram of the ICT gastric gavage method used in mice. (B) Tumors were removed and subjected to ICT gastric gavage for 14 days. The data are presented as the mean ± SD; $n = 6$ mice per group. (C, D) The tumor volume was dynamically observed weekly until death or when it reached 2000 mm^3. Tumor weight was measured on Day 21. The data are presented as the mean ± SD: $^{**}P < 0.01$, $^{****}P < 0.0001$, $n = 6$ mice per group. (E) Kaplan−Meier curves showing the overall survival of mice after treatment with different doses of ICT; $n = 6$ mice per group. (F) Immunohistochemical staining of $CD3^+$, $CD4^+$, and $CD8^+$ T cells in tumors treated with ICT (30 mg/kg) and in control groups; scale bars, 100 μm. (G−I) Flow cytometric analysis of T-cell subpopulations, checkpoints, effector molecules, NK cells, DCs, and macrophages isolated from tumors treated with or without ICT (30 mg/kg). The data are presented as the mean ± SD; $^{*}P < 0.05$, $^{**}P < 0.01$, $^{***}P < 0.001$; $n = 6$ mice per group. (J) Flow cytometric analysis of neutrophils in tumors treated with or without ICT (30 mg/kg). The data are presented as the mean ± SD, $^{**}P < 0.01$, $n = 6$ mice per group. (K) Immunohistochemical staining of Ly-$6G^+$ neutrophils in the tumors treated with ICT (30 mg/kg) and in the control group; scale bars, 100 μm. (L) *In vivo* imaging of metastatic foci in the lungs of mice intravenously injected with 3×10^5 MB49-luc cells and treated with or without ICT (30 mg/kg). The cells were imaged on Day 21. (M) HE staining revealed metastatic foci in the lungs of mice after neutrophil depletion and treatment with or without ICT (30 mg/kg). Lung nodules were observed, and the data are presented as the mean ± SD: $^{***}P < 0.001$, $n = 5$ mice per group. (N) Numbers of lung nodules were detected after $CD4^+$ T cells or $CD8^+$ T cells were depleted separately and treated with or without ICT (30 mg/kg).

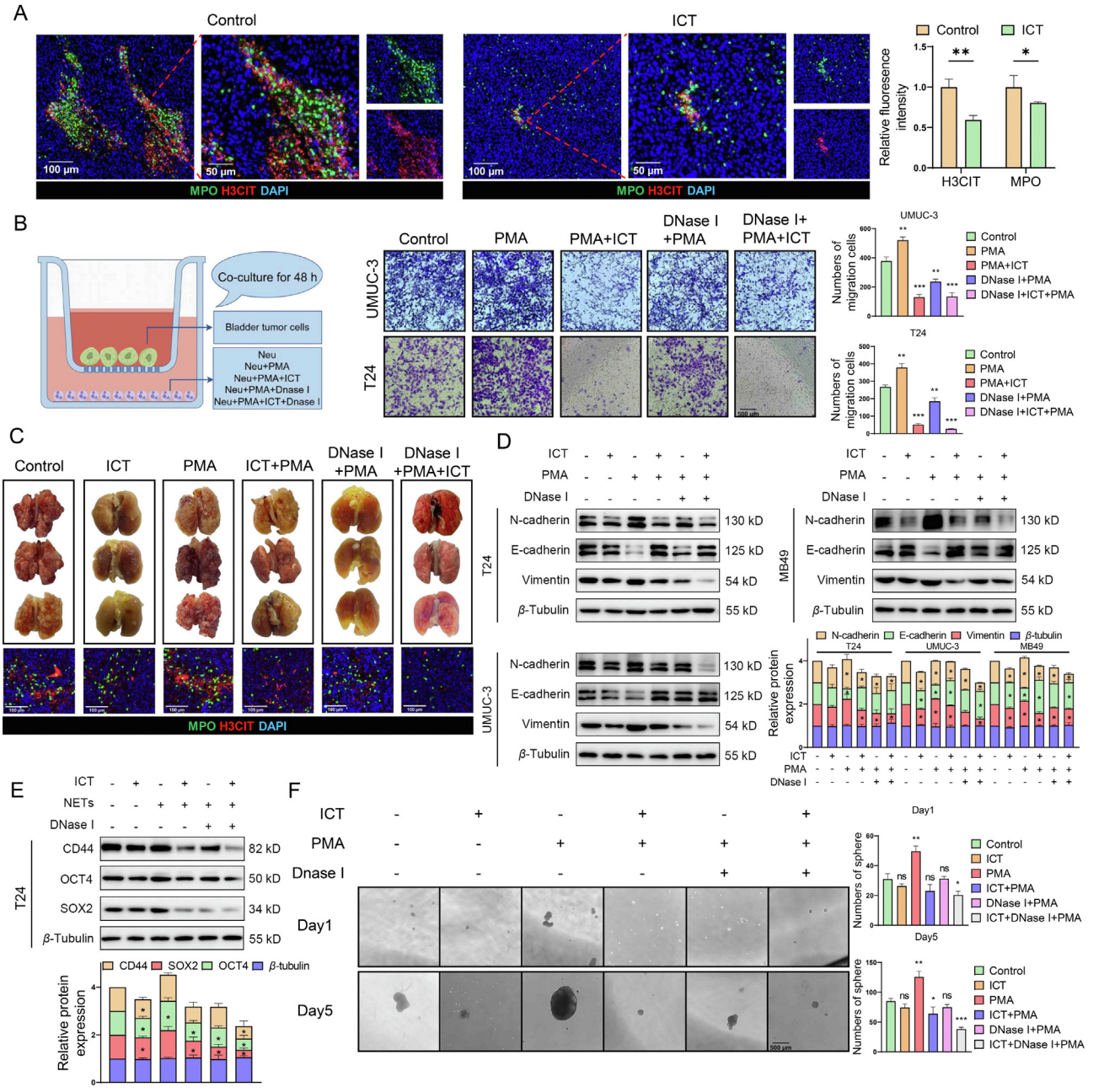

Figure 3 ICT inhibits NET-induced tumor metastasis and stemness. (A) Immunofluorescence staining of the intratumor area and distribution of MPO (green) and H3CIT (red) in tumors treated with or without ICT (30 mg/kg). DAPI (blue) was used for nuclear staining. Scale bars, 200 μm, 50 μm. (B) Schematic diagram and representative images of the Transwell assay with cocultured tumor cells and pretreated neutrophils for 48 h. The results are presented as the mean ± SD, $^{**}P < 0.01$, $^{***}P < 0.001$. (C) Lung metastasis of mice treated with ICT, PMA, or DNase I. Scale bar, 100 mm. Immunofluorescence staining of metastatic tumors showing the distribution of MPO (green), H3CIT (red), and nuclei (DAPI). Scale bars, 100 μm. (D) WB assays demonstrating the effects of ICT alone or in combination with PMA and DNase I on the human urothelial cancer cell lines T24 and UMUC-3 and the murine urothelial cancer cell line MB49. Relative protein expression levels are quantitively graphed. The data are presented as the mean ± SD, $^{*}P < 0.05$. (E) WB assays show changes in the expression of tumor stemness-related proteins. (F) Spheroid growth of T24 cells cultured in medium supplemented with neutrophils pretreated with ICT, PMA, or DNase I. Scale bar, 500 mm. The data are presented as the mean ± SD; $^{*}P < 0.05$, $^{**}P < 0.01$, $^{***}P < 0.001$.

analysis showing a concentration-dependent decrease in the expression of PADI2 and its downstream target H3CIT (Fig. 4G). Biacore analysis provided further evidence of a direct interaction between ICT and PADI2 (Fig. 4H). Suicidal NETosis induced by PMA is a predominant form of NETosis within the tumor microenvironment and was inhibited by ICT (Fig. 4J, Fig. S4E). The production of reactive oxygen species (ROS) is one of the characteristic features of suicidal NETosis and was inhibited by ICT in neutrophils (Fig. 4K). By combining the GSEA results (Fig. 4I) and subsequent pathway analysis, we revealed that ICT suppressed the activation of MAPK signaling pathways, specifically the PI3K/AKT pathway and MEK/ERK/p38 pathway, while

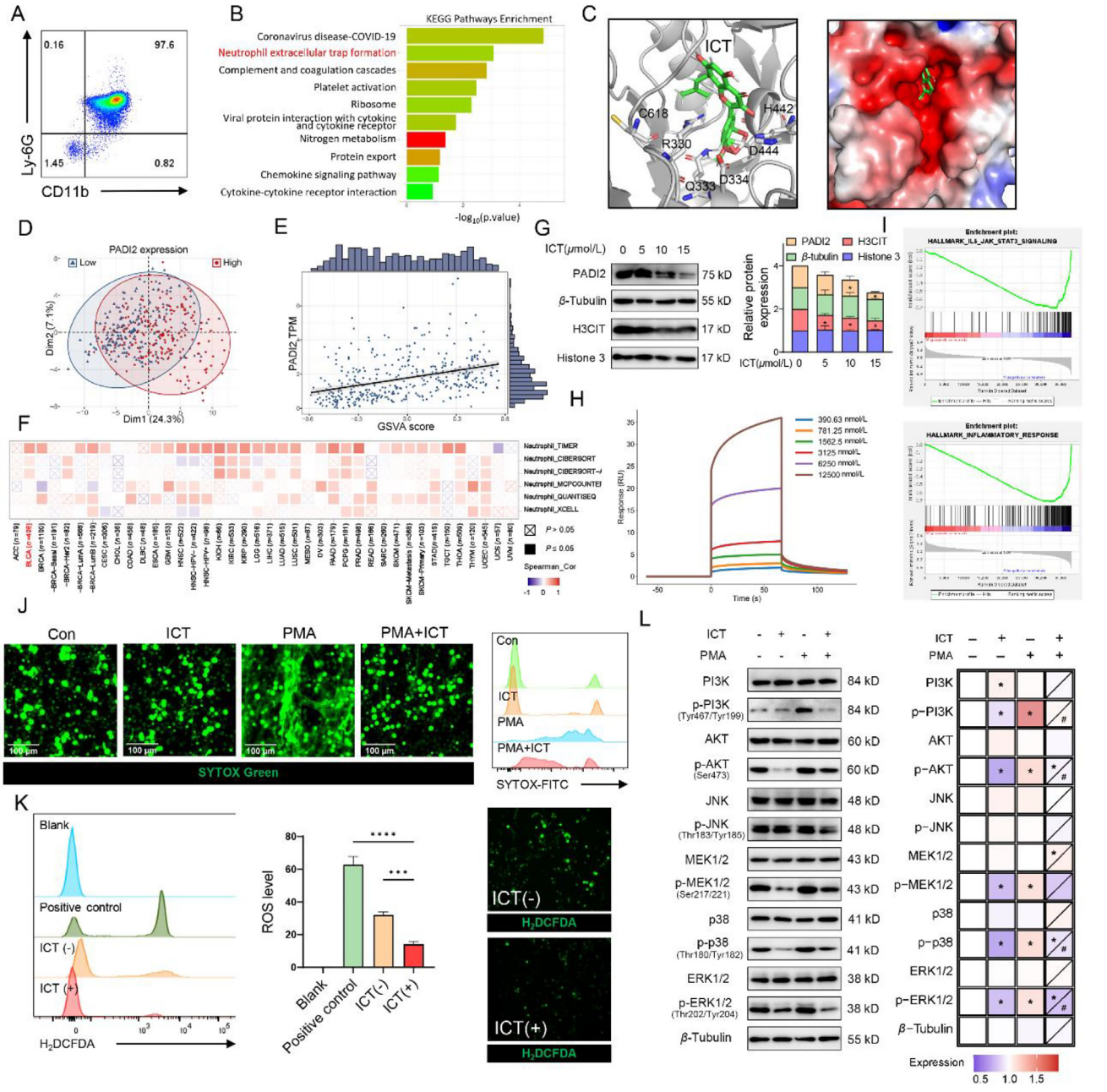

Figure 4 ICT inhibits PADI2 expression and NETosis. (A) Flow cytometry was used to validate the purity of isolated $CD45^{+}CD11b^{+}Ly\text{-}6G^{+}$ neutrophils. (B) KEGG functional enrichment analysis was conducted on RNA-sequencing data from neutrophils treated with or without ICT. (C) ICT-PADI2 interaction sites in the pocket. (D) PCA was performed to determine the effect of PADI2 on the expression of NET-associated genes. (E) Relationship between the expression of PADI2 and the GSVA score of NET-associated genes. (F) Pancancer analysis revealed the relationship between PADI2 and different tumors. (G) WB assays showing the effects of ICT on PADI2 and H3CIT. Relative protein expression is quantitively graphed. The data are presented as the mean ± SD; $^{*}P < 0.05$. (H) The interaction between ICT and PADI2 was detected by surface plasmon resonance. K_D (M) $= 6.160 \times 10^{-5}$. (I) GSEA was performed to examine potential pathways and responses involving PADI2. (J) Representative images and flow cytometry images of SYTOX Green (FITC)-stained dead neutrophils and NETs after 4 h of treatment with PMA or ICT. (K) ROS analysis of neutrophils treated with ICT. (L) WB assays showing NETosis-associated pathways in cells treated with ICT. Relative protein expression is quantitively graphed. The data are presented as the mean ± SD: $^{*}P < 0.05$, *versus* blank; $^{\#}P < 0.05$, *versus* $PMA^{+}ICT^{-}$.

its effect on the JNK signaling pathway was not significant (Fig. 4L). During suicidal NETosis, ROS also increase the permeability of the nuclear membrane and promote chromatin decondensation, which results in elevated expression of NE and MPO. Western blot results confirmed that ICT inhibited MPO expression during this process (Fig. S4F). Additionally, the expression of other proteins in NETs that promote tumor progression and metastasis, such as MMP9, VEGFA, and HMGB1, was also downregulated by ICT at higher concentrations (Fig. S4F). In conclusion, these results suggest that ICT may

suppress NET formation by inhibiting suicidal NETosis and PADI2-mediated histone citrullination, which provides novel insight into the anticancer mechanisms of ICT.

3.5. ICT suppresses neutrophil infiltration by inhibiting PADI2-mediated histone citrullination and the positive feedback loop for IL-6/JAK2/STAT3 signaling

Previous studies have demonstrated that ICT not only inhibits NET formation but also suppresses neutrophil infiltration. To further dissect the mechanism underlying the inhibition of neutrophil infiltration by ICT, tumor cell supernatants treated with ICT for 48 h were analyzed using a cytokine array, which revealed a downregulation of several cytokines associated with neutrophil recruitment (Fig. 5A). Functional enrichment analysis suggested that this inhibition might be associated with the JAK/STAT signaling pathway (Fig. 5B). To ascertain whether the suppression of neutrophil recruitment by ICT was due to the inhibition of chemokine release by tumor cells, an *in vitro* neutrophil-tumor coculture system was established. After treatment with increasing concentrations of ICT, the number of neutrophils remaining in the upper chamber also increased, and the number of those recruited to the lower chamber decreased (Fig. 5C−D). Histone citrullination can facilitate transcription factor binding and promote transcription; hence, qPCR was performed by ICT to assess the regulation of neutrophil-related gene transcription. The results indicated that the transcription of IL-6 and IL-8 was consistently suppressed across different tumor cell lines (Fig. 5E), which was further proven by ELISA, which demonstrated a concentration-dependent decrease in IL-6 release (Fig. 5F). Given that PADI2-mediated histone citrullination can enhance the transcription of IL-6, the combination of ICT with the PADI2 inhibitor AFM32a was used for further mechanistic exploration. ICT was revealed to inhibit the intratumoral expression of PADI2 and, consequently, PADI2-mediated H3CIT. AFM32a exerted a synergistic effect with ICT. Moreover, significant suppression of JAK2/STAT3 was also observed (Fig. 5H). *In vivo* experiments demonstrated that ICT exhibited inhibitory effects on tumors superior to those of AFM32a (Fig. 5G). Since IL-6 can activate the JAK2/STAT3 signaling pathway, a rescue experiment with recombinant IL-6 (rIL-6) was conducted. The addition of rIL-6 upregulated the activation of JAK2/STAT3, which could be reversed by ICT. Concurrently, IL-8, a downstream transcriptional target of activated JAK2/STAT3, was also regulated (Fig. 5I). Taken together, ICT similarly suppresses PADI2 expression within tumors, and the inhibition of PADI2 expression leads to reduced histone citrullination within tumor cells, causing a downstream decrease in IL-6 transcription and impeding neutrophil recruitment. Decreased IL-6 levels could further inhibit the JAK2/STAT3 signaling pathway, thus disrupting the positive transcriptional feedback loop of IL-6.

3.6. PADI2-mediated NETs possess prognostic value for urothelial cancer

To validate that PADI2-mediated NETs are a prognostic biomarker in urothelial cancer, we collected tissue and blood samples from patients with urothelial carcinoma for correlation analysis (Fig. 6A). Immunohistochemical staining for PADI2, the neutrophil marker CD66b, and the NET marker H3CIT was also performed (Fig. 6B). According to a retrospective analysis of 195 evaluable patients, high intratumoral expression of CD66b was associated with poor clinical prognosis (Supporting Information Table S3). Additionally, CD66b was found to be related to higher tumor grade and advanced pathological stage, while H3CIT was not, possibly due to its native expression within the tumor (Fig. 6C). Combined analysis of the NET markers CD66b and H3CIT revealed that patients with high expression of both markers had the worst prognosis (Fig. 6D). Further analysis of the correlations between neutrophils, NETs, and chemotherapy sensitivity showed that neutrophil infiltration was associated with chemoresistance (Fig. 6E). To clarify the relationship between NETs and tumor progression or recurrence, ELISA was performed using the peripheral blood serum of 40 patients, revealing that MPO-DNA levels were greater in patients with muscle-invasive bladder cancer (MIBC) than in those with nonmuscle invasive bladder cancer (NMIBC, Fig. 6F). Follow-up of patients after transurethral resection of bladder tumor (TURBT) surgery also indicated that patients with increased plasma MPO-DNA after surgery tended to experience recurrence (Fig. 6G). These results highlight the potential of neutrophils and NET-related components in predicting the recurrence and progression of urothelial cancer. Although the intratumoral expression of H3CIT may not be a reliable prognostic indicator alone, combining CD66b and H3CIT could significantly improve the prediction of tumor prognosis.

3.7. ICT synergizes with anti-PD-1 immunotherapy to counteract T-cell exhaustion induced by NETs

Previous research has confirmed that neutrophils and NETs can suppress the antitumor function of T cells within the tumor microenvironment, inducing T-cell exhaustion and leading to immune escape. Therefore, we analyzed the relationships among neutrophils, NETs, and T-cell exhaustion in tumors (Fig. 7A). Correlation analysis revealed that neutrophil infiltration and NETs in tumors were related to increased T-cell infiltration. However, the expression of PD-1 was also elevated (Fig. 7B). Fresh tissue samples from 24 patients with urothelial cancer were collected and digested into single-cell suspensions. Flow cytometry analysis of tumor-infiltrating immune cells was performed, and the results indicated that CD66b infiltration was correlated with upregulated PD-1 and $CD8^+$TIM3 expression, suggesting an association between high neutrophil infiltration and immune exhaustion (Fig. 7C and D). Having confirmed that ICT can inhibit neutrophil infiltration and NET formation, we further explored whether ICT could be used in combination with anti-PD1 therapy to reverse T-cell exhaustion. In an animal model investigating the efficacy of the combination (Fig. 7E), the results demonstrated that ICT combined with anti-PD-1 treatment significantly reduced tumor growth (Fig. 7F) and improved the prognosis of mice (Fig. 7G). Immunohistochemical analysis of the tumors revealed reduced Ki67 expression and increased infiltration of $CD4^+$ and $CD8^+$ T cells (Fig. 7H). These results thus confirm that ICT can reshape the immune microenvironment by inhibiting neutrophil and NET formation, thereby reversing tumor immune escape. The combined application of ICT and anti-PD-1 immunotherapy can act synergistically to enhance antitumor immunity.

3.8. Data availability statement

The data that support the findings of this study are available from the corresponding author upon reasonable request.

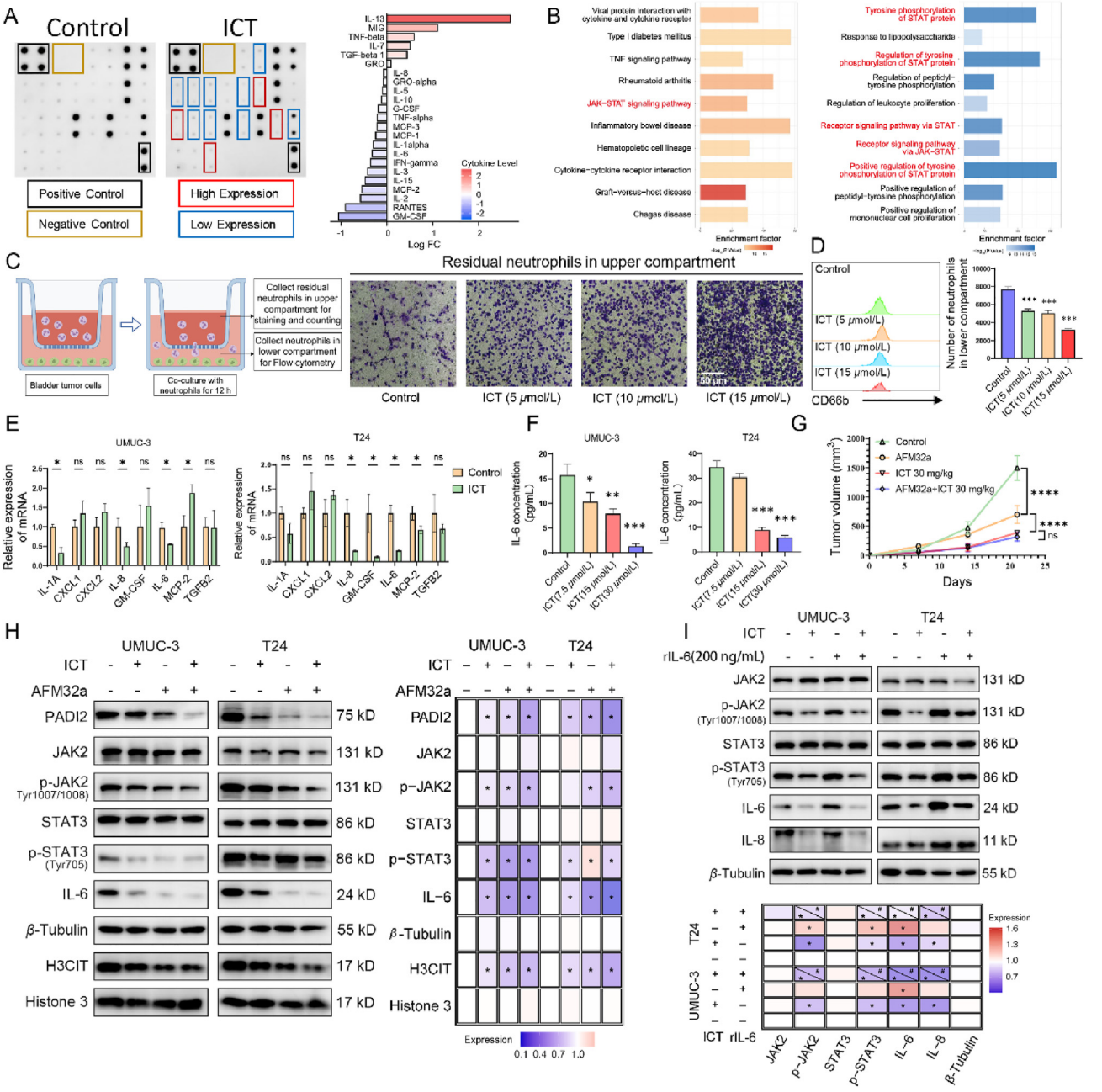

Figure 5 ICT inhibits tumor recruitment to neutrophils. (A) Cytokine array analyses of UMUC-3 media after 24 h of treatment with ICT. (B) KEGG (left) and GO (right) functional enrichment analysis of cytokines. (C) Schematic diagram and representative images of the Transwell assay in which neutrophils and pretreated tumor cells were cocultured for 12 h. (D) The number of neutrophils in the lower compartment was examined by flow cytometry. The data are presented as the mean ± SD; $^{***}P < 0.001$. (E) RNA expression in UMUC-3 and T24 cells treated with ICT was detected by RT-qPCR. The data are presented as the mean ± SD, $^{*}P < 0.05$. (F) ELISAs showing IL-6 release from UMUC-3 and T24 cells following ICT addition. The data are presented as the mean ± SD; $^{*}P < 0.05$, $^{**}P < 0.01$, $^{***}P < 0.001$. (G) The tumor volume was dynamically observed weekly after treatment with ICT, AFM32a, and AFM32a + ICT. $^{****}P < 0.0001$, $n = 6$ mice per group. (H) WB assays show the protein expression regulated by ICT and AFM32a (a PADI2 inhibitor). Relative protein expression is quantitively graphed. The data are presented as the mean ± SD; $^{*}P < 0.05$. (I) WB assays show the protein expression regulated by ICT and rIL-6. Relative protein expression is quantitively graphed. The data are presented as the means ± SDs; $^{*}P < 0.05$, *versus* the blank; $^{\#}P < 0.05$, *versus* the rIL-6^{+}ICT^{-} group.

4. Discussion

The treatment of diseases is greatly aided by traditional Chinese medicine (TCM), which has a long history. TCM is becoming an increasingly important resource for new drug innovation[29]. In fact, numerous TCM herbal extracts, which have passed clinical trials, are used to treat diseases such as diabetes, cardiovascular disease, and leukemia[30]. The importance of TCM in cancer treatment is also increasingly recognized. TCM herbal extracts have been proven to inhibit various cancers by modulating multiple cellular pathways.

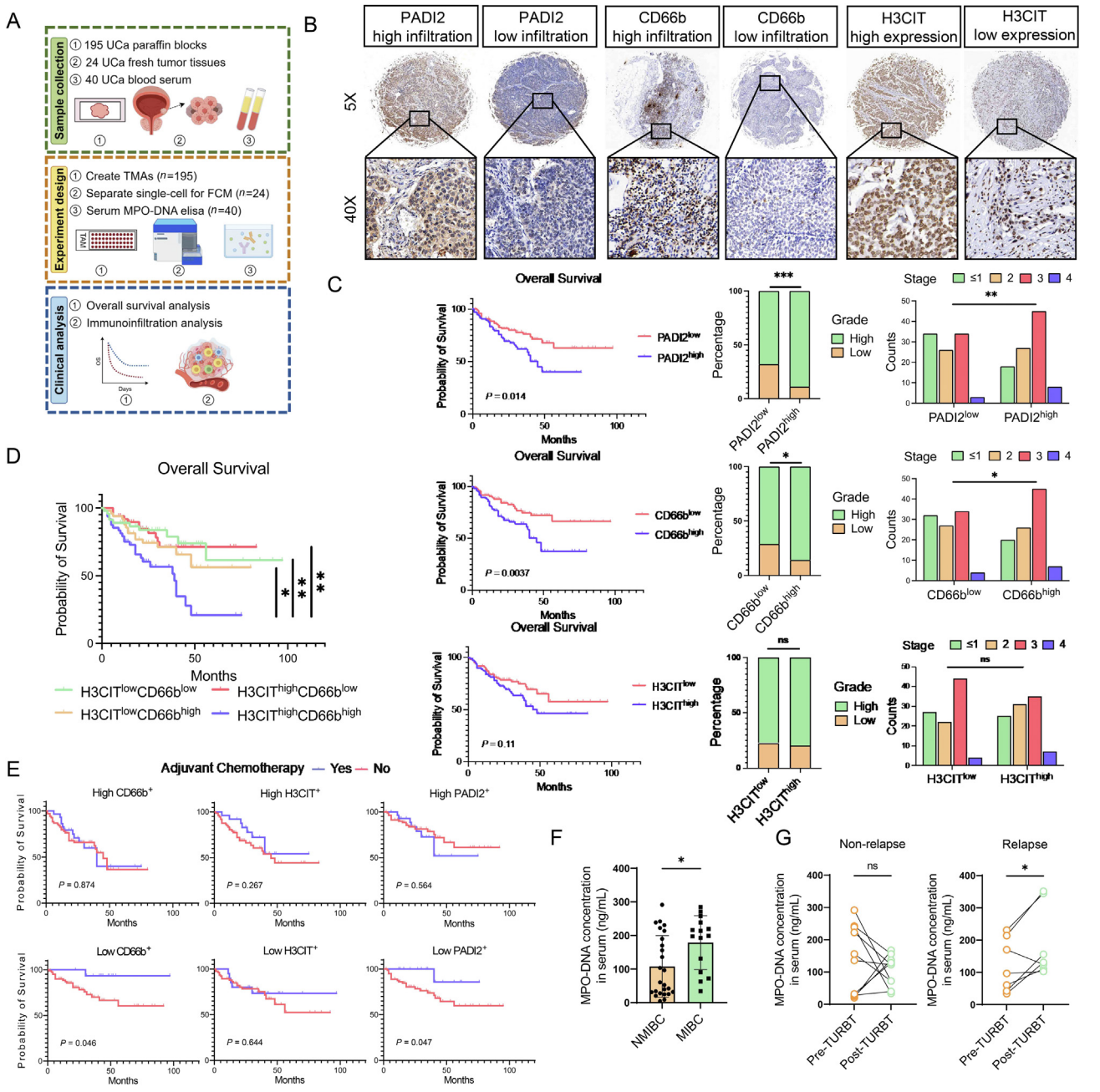

Figure 6 PADI2 expression is correlated with NETs and poor prognosis in UCa patients. (A) Overview of the experimental design and clinical data analysis workflow for the clinical study. (B) Representative images of IHC staining illustrating intratumoral PADI2, CD66b, and H3CIT expression based on low and high staining intensities. (C) OS, grade, and stage of UCa patients based on the median PADI2, CD66b, and H3CIT expression scores. (D) OS of UCa patients based on the median score of CD66b and H3CIT combination expression. (E) The predictive value of CD66b, H3CIT, and PADI2 infiltration levels for adjuvant chemotherapy benefit. (F, G) The serum concentration of the NET marker MPO-DNA was detected by ELISA. The data are presented as the mean ± SD; $^*P < 0.05$.

The main Epimedium extract, icariin (ICA), is converted by the body into icaritin (ICT), which has biological benefits[4]. In addition to its diverse biological effects, such as modulating adaptive immunity and offering anti-hepatotoxicity and antioxidant properties, ICT also has antitumor effects on various cancers. ICT targets the Wnt/β-catenin pathway in ovarian cancer[31] to hinder tumor growth, inhibits cellular autophagy in breast cancer, reduces chemotherapy resistance[7], and, combined with doxorubicin in hepatocellular carcinoma, remodels the tumor's immune-suppressive environment to induce cell death[4]. However, there is a lack of studies on the application of ICT in urothelial cancer. In this study, we conducted a thorough investigation into the mechanism of immune checkpoint therapy (ICT) in urothelial carcinoma, demonstrating its capacity to suppress tumor growth and trigger apoptosis while having little *in vitro* impact on tumor invasion.

Nonetheless, *in vivo* studies revealed that ICT could inhibit tumor invasion and metastasis, leading to speculation about whether ICT's inhibition of tumor invasion and metastasis is

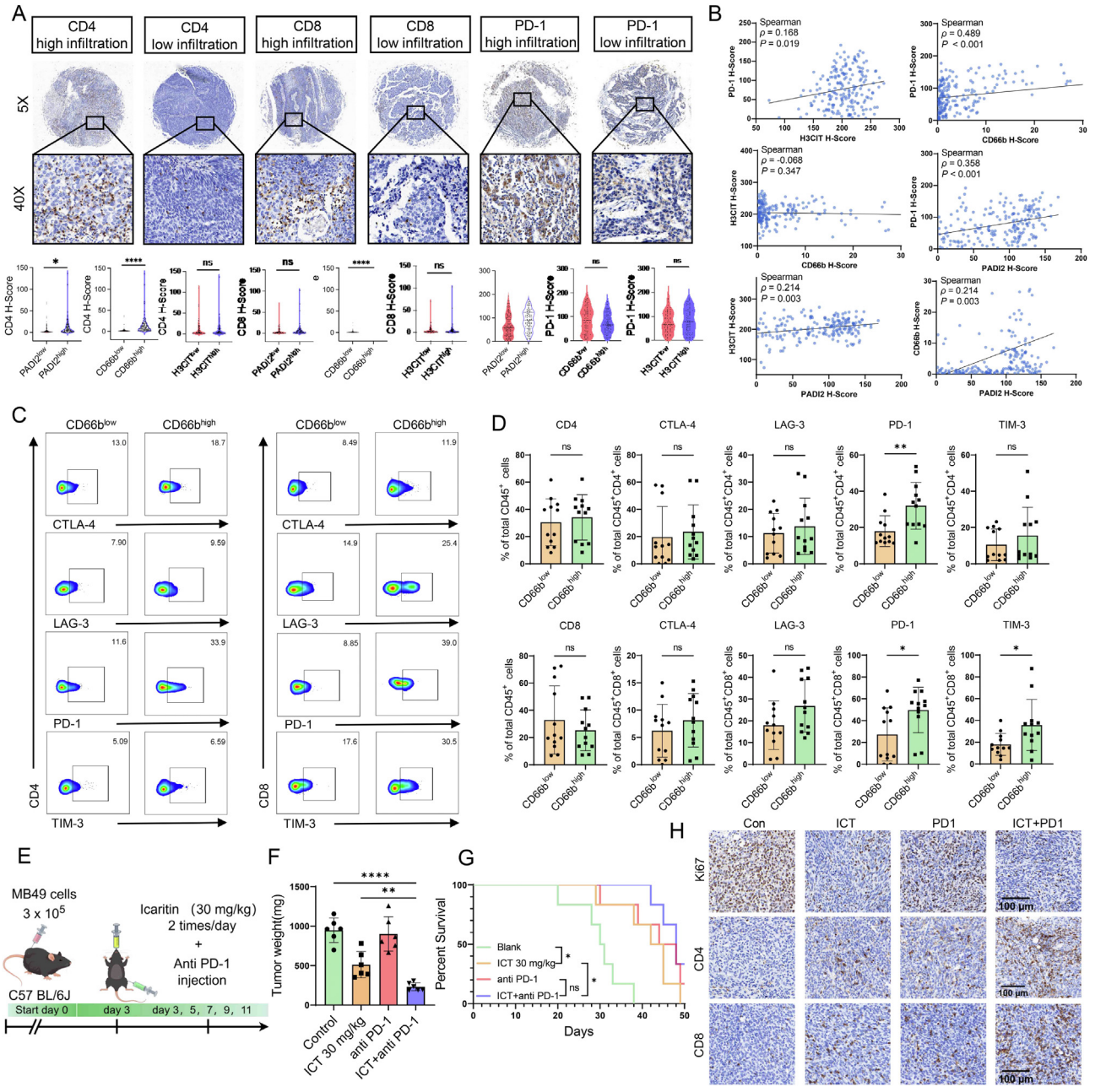

Figure 7 ICT and anti-PD-1 immunotherapy exerted synergistic antitumor effects. (A) Representative IHC staining images illustrating intratumoral CD4, CD8, and PD-1 infiltration based on low and high staining intensities. The data are presented as the mean ± SD; $^{*}P < 0.05$, $^{***}P < 0.001$, $^{****}P < 0.0001$. (B) Correlation of PD-1, CD66b, H3CIT, and PADI2 expression in UCa. (C, D) Flow cytometric analysis of immune checkpoint expression in $CD4^+$ and $CD8^+$ T cells from fresh human UCa tissues. The data are presented as the mean ± SD: $^{*}P < 0.05$, $CD66b^{low}$ *versus* $CD66b^{high}$. (E) Schematic diagram of the ICT and anti-PD-1 combination therapy. (F) The weights of the tumors were observed. $n = 6$ mice per group, $^{**}P < 0.01$, $^{****}P < 0.0001$. (G) Kaplan−Meier curves illustrate the survival of the mice. (H) Immunohistochemical staining of Ki67 and $CD4^+$ and $CD8^+$ T cells in murine tumors. Scale bars, 100 μm.

related to other factors in the tumor microenvironment. Previous studies have shown that the antitumor effect of ICT is often linked to its regulation of the tumor immune microenvironment (TME). ICT increases the number of tumor-infiltrating $CD4^+$ and $CD8^+$ T cells in the TME by decreasing the levels of immunosuppressive molecules (PD-L1 and IL-10) and cellular subsets (MDSCs, Tregs, and macrophages), enhancing antitumor immunity[8-11]. Consequently, we quantitatively analyzed immune cell subpopulations in a murine tumor model using flow cytometry and discovered that ICT increased T-cell infiltration and decreased neutrophil infiltration. Subsequent research revealed that controlling neutrophil infiltration was the means by which ICTs inhibited tumor spread in people. Neutrophils were thus the subject of our subsequent studies.

Neutrophils are the human body's most abundant innate immune effector cells. Neutrophils, as a crucial component of the TME, play dual roles in tumor regulation. In the early stages of tumors, numerous recruited and activated neutrophils in the TME

directly interact with and produce reactive oxygen species (ROS), which kill tumor cells[32]. Additionally, some neutrophils are thought to exhibit an antigen-presenting cell (APC) phenotype, activating $CD4^+$ T and $CD8^+$ T cells to proliferate and eliminate tumor cells[33]. However, neutrophils exhibit the opposite effect in the progression stage of the tumor. The most significant protumor effect of neutrophils is attributed to tumor immune suppression. Through mediators such as ROS, NOS, and arginase 1 (ARG1), neutrophils in the TME can suppress T-cell activation[34].

Furthermore, some neutrophils can express PD-L1 on their surface, which causes T-cell death and immunological evasion[35]. In addition to suppressing tumor immunity, tumor-associated neutrophils (TANs), which are remodeled in the TME, can release NETs, which promote tumor proliferation and invasion *via* a unique death mode called NETosis[36]. Various endogenous or exogenous stimuli initiate this process, which begins with the activation of the MEK-ERK signaling pathway, leading to the induction of ROS that trigger the myeloperoxidase (MPO) pathway. Subsequently, MPO mediates the oxidative activation of neutrophil elastase (NE), which degrades the actin cytoskeleton in the cytoplasm and moves to the nucleus to promote chromatin depolymerization; simultaneously, MPO binds to DEK and activates histone citrullination *via* protein-arginine deiminase (PADI) family proteins 2/4, furthering chromatin depolymerization. The rupture of neutrophil cellular membranes results in the release of NET structures. Clinical evidence indicates that elevated NETs correlate with poor prognosis in various tumors, including sarcoma, melanocytoma, and hepatocellular carcinoma[17,20,21]. It has also been demonstrated that NETs can promote epithelial−mesenchymal transition (EMT) in endothelial cells[25]. However, research on the role of NETs in urothelial cancer regulation is relatively limited. In this study, we demonstrated for the first time that ICT can inhibit the generation of NETs *via* two pathways: (1) ICT inhibits the MAPK signaling pathway, thereby reducing ROS generation and preventing NETosis activation, and (2) ICT binds to PADI2, inhibiting its expression and thus inhibiting histone citrulline modification. This work fills a gap in the literature by demonstrating the potential of ICT as a targeted NET inhibitor in the absence of a functional inhibitor that targets NETs.

The function of ICT in preventing tumor-induced neutrophil recruitment, which is also dependent on ICT-mediated prevention of PADI2-mediated citrullinated histone modifications in tumors, is another important discovery of this work. Citrulline modification decreases the affinity of histones for DNA, increasing the accessibility of DNA to binding transcription factors and enhancing transcription. Cytokine microarray and RT-qPCR analyses of ICT-treated tumor cell supernatants revealed reduced expression of neutrophil recruitment-related proteins, including GM-CSF, IL-6, CCL5, MCP-1, MCP-2, and IL-8. Additionally, cytokines such as GM-CSF and IL-6 activate the JAK2/STAT3 signaling pathway, enhancing their transcription and creating a positive feedback loop. This inhibitory effect of ICT can be reversed by the addition of rIL-6. Concurrently, combined with the analysis of tissue microarrays and clinical prognoses of UCa patients, we found that high neutrophil infiltration corresponds with a worse prognosis and reduced sensitivity to adjuvant chemotherapy. Flow cytometry analysis of fresh patient tissues further confirmed a correlation between high neutrophil infiltration and T-cell functional exhaustion. This prognostic difference is associated with neutrophil-mediated immune escape. However, variations in the expression of H3CIT, a NET marker, did not correlate with patient prognosis, leading to the hypothesis that this is due to the low specificity of H3CIT, as neutrophils are not the only cells expressing H3CIT in the tumor microenvironment. Analysis of CD66b alongside H3CIT revealed a significant correlation with prognosis.

5. Conclusions

In conclusion, our investigation revealed that while ICT suppresses neutrophil infiltration and NET synthesis, significantly decreasing tumor spread and progression, neutrophils and NETs play inhibitory roles in the tumor immune microenvironment of UCa patients. Additionally, the combination of ICT with anti-PD-1 immunotherapy has synergistic effects, suggesting a potential therapeutic strategy for UCa patients.

Acknowledgments

We would like to thank the bladder tumour patients for their willingness to further research through study participation. This work was supported in part by grants from National Natural Science Foundation of China (No.82373222, No.82202970), Leading Talent Program by Shanghai Municipal Health Commission (2022LJ008, China), Shanghai Shenkang Hospital Development Center (SHDC12021104, China), Science and Technology Commission of Shanghai Municipality (22Y21900200 & 22YF1404300, China).

Author contributions

Zezhong Mou: Investigation, Methodology, Visualization, Writing − original draft. Yiling Chen: Investigation, Methodology, Visualization, Writing − original draft. Jinzhong Hu: Methodology, Writing − original draft. Yun Hu: Methodology. Lujia Zou: Investigation. Xinan Chen: Investigation. Shenghua Liu: Investigation. Qiuping Yin: Investigation. Jian Gong: Investigation. Shuchen Li: Investigation, Visualization. Shanhua Mao: Conceptualization, Writing − review & editing, Supervision. Chenyang Xu: Conceptualization, Funding acquisition, Investigation, Supervision. Haowen Jiang: Conceptualization, Funding acquisition, Supervision, Writing − review & editing.

Conflicts of interest

The authors have declared that no conflict of interest exists.

Appendix A. Supporting information

Supporting information to this article can be found online at https://doi.org/10.1016/j.apsb.2024.06.029.

References

1. Sanli O, Dobruch J, Knowles MA, Burger M, Alemozaffar M, Nielsen ME, et al. Bladder cancer. *Nat Rev Dis Primers* 2017;**3**:17022.
2. Siegel RL, Miller KD, Wagle NS, Jemal A. Cancer statistics, 2023. *CA Cancer J Clin* 2023;**73**:17−48.
3. Zheng RS, Chen R, Han BF, Wang SM, Li L, Sun KX, et al. Cancer incidence and mortality in China, 2022. *Zhonghua Zhong Liu Za Zhi* 2024;**46**:221−31.
4. Bi Z, Zhang W, Yan X. Anti-inflammatory and immunoregulatory effects of icariin and icaritin. *Biomed Pharmacother* 2022;**151**:113180.
5. Wang S, Ma J, Zeng Y, Zhou G, Wang Y, Zhou W, et al. Icariin, an up-and-coming bioactive compound against neurological diseases:

network pharmacology-based study and literature review. *Drug Des Devel Ther* 2021;**15**:3619−41.
6. Chen C, Wang S, Wang N, Zheng Y, Zhou J, Hong M, et al. Icariin inhibits prostate cancer bone metastasis and destruction *via* suppressing TAM/CCL5-mediated osteoclastogenesis. *Phytomedicine* 2023;**120**:155076.
7. Cheng X, Tan S, Duan F, Yuan Q, Li Q, Deng G. Icariin induces apoptosis by suppressing autophagy in tamoxifen-resistant breast cancer cell line MCF-7/TAM. *Breast Cancer* 2019;**26**:766−75.
8. Song L, Chen X, Mi L, Liu C, Zhu S, Yang T, et al. Icariin-induced inhibition of SIRT6/NF-κB triggers redox mediated apoptosis and enhances anti-tumor immunity in triple-negative breast cancer. *Cancer Sci* 2020;**111**:4242−56.
9. Zhou J, Wu J, Chen X, Fortenbery N, Eksioglu E, Kodumudi KN, et al. Icariin and its derivative, ICT, exert anti-inflammatory, anti-tumor effects, and modulate myeloid derived suppressive cells (MDSCs) functions. *Int Immunopharmacol* 2011;**11**:890−8.
10. Bailly C. Molecular and cellular basis of the anticancer activity of the prenylated flavonoid icaritin in hepatocellular carcinoma. *Chem Biol Interact* 2020;**325**:109124.
11. Huang C, Li Z, Zhu J, Chen X, Hao Y, Yang R, et al. Systems pharmacology dissection of epimedium targeting tumor microenvironment to enhance cytotoxic T lymphocyte responses in lung cancer. *Aging (Albany NY)* 2021;**13**:2912−40.
12. Liew PX, Kubes P. The neutrophil's role during health and disease. *Physiol Rev* 2019;**99**:1223−48.
13. Zhang H, Wang Y, Qu M, Li W, Wu D, Cata JP, et al. Neutrophil, neutrophil extracellular traps and endothelial cell dysfunction in sepsis. *Clin Transl Med* 2023;**13**:e1170.
14. Lu H, Lin J, Xu C, Sun M, Zuo K, Zhang X, et al. Cyclosporine modulates neutrophil functions via the SIRT6-HIF-1α-glycolysis axis to alleviate severe ulcerative colitis. *Clin Transl Med* 2021;**11**:e334.
15. Peng H, Wu X, Liu S, He M, Tang C, Wen Y, et al. Cellular dynamics in tumour microenvironment along with lung cancer progression underscore spatial and evolutionary heterogeneity of neutrophil. *Clin Transl Med* 2023;**13**:e1340.
16. Quail DF, Amulic B, Aziz M, Barnes BJ, Eruslanov E, Fridlender ZG, et al. Neutrophil phenotypes and functions in cancer: a consensus statement. *J Exp Med* 2022;**219**:e20220011.
17. Tohme S, Yazdani HO, Al-Khafaji AB, Chidi AP, Loughran P, Mowen K, et al. Neutrophil extracellular traps promote the development and progression of liver metastases after surgical stress. *Cancer Res* 2016;**76**:1367−80.
18. Adrover JM, McDowell SAC, He XY, Quail DF, Egeblad M. NETworking with cancer: the bidirectional interplay between cancer and neutrophil extracellular traps. *Cancer Cell* 2023;**41**:505−26.
19. Wang W, Zhang J, Zheng N, Li L, Wang X, Zeng Y. The role of neutrophil extracellular traps in cancer metastasis. *Clin Transl Med* 2020;**10**:e126.
20. Berger-Achituv S, Brinkmann V, Abed UA, Kühn LI, Ben-Ezra J, Elhasid R, et al. A proposed role for neutrophil extracellular traps in cancer immunoediting. *Front Immunol* 2013;**4**:48.
21. Schedel F, Mayer-Hain S, Pappelbaum KI, Metze D, Stock M, Goerge T, et al. Evidence and impact of neutrophil extracellular traps in malignant melanoma. *Pigment Cel Melanoma Res* 2020;**33**:63−73.
22. Yin Y, Dai H, Sun X, Xi Z, Zhang J, Pan Y, et al. HRG inhibits liver cancer lung metastasis by suppressing neutrophil extracellular trap formation. *Clin Transl Med* 2023;**13**:e1283.
23. Cai J, Xue R, Yue Z, Zhang Z, He L, Li H, et al. Neutrophil to lymphocyte ratio as a predictor for treatment of radiation-induced brain necrosis with bevacizumab in nasopharyngeal carcinoma patients. *Clin Transl Med* 2022;**12**:e583.
24. Shan ZG, Chen J, Liu JS, Zhang JY, Wang TT, Teng YS, et al. Activated neutrophils polarize protumorigenic interleukin-17A-producing T helper subsets through TNF-α-B7-H2-dependent pathway in human gastric cancer. *Clin Transl Med* 2021;**11**:e484.
25. Cristinziano L, Modestino L, Antonelli A, Marone G, Simon HU, Varricchi G, et al. Neutrophil extracellular traps in cancer. *Semin Cancer Biol* 2022;**79**:91−104.
26. Teijeira Á, Garasa S, Gato M, Alfaro C, Migueliz I, Cirella A, et al. CXCR1 and CXCR2 chemokine receptor agonists produced by tumors induce neutrophil extracellular traps that interfere with immune cytotoxicity. *Immunity* 2020;**52**:856−871.e8.
27. Mou Z, Chen Y, Zhang Z, Chen X, Hu Y, Zou L, et al. Cryoablation inhibits the recurrence and progression of bladder cancer by enhancing tumour-specific immunity. *Clin Transl Med* 2023;**13**:e1255.
28. Mou Z, Yang C, Zhang Z, Wu S, Xu C, Cheng Z, et al. Transcriptomic analysis of glycolysis-related genes reveals an independent signature of bladder carcinoma. *Front Genet* 2020;**11**:566918.
29. Tu Y. Artemisinin-a gift from traditional Chinese medicine to the world (nobel lecture). *Angew Chem Int Ed Engl* 2016;**55**:10210−26.
30. Wang J, Wong YK, Liao F. What has traditional Chinese medicine delivered for modern medicine?. *Expert Rev Mol Med* 2018;**20**:e4.
31. Fu Y, Liu H, Long M, Song L, Meng Z, Lin S, et al. Icariin attenuates the tumor growth by targeting miR-1-3p/TNKS2/Wnt/β-catenin signaling axis in ovarian cancer. *Front Oncol* 2022;**12**:940926.
32. Mahiddine K, Blaisdell A, Ma S, Créquer-Grandhomme A, Lowell CA, Erlebacher A. Relief of tumor hypoxia unleashes the tumoricidal potential of neutrophils. *J Clin Invest* 2020;**130**:389−403.
33. Singhal S, Bhojnagarwala PS, O'Brien S, Moon EK, Garfall AL, Rao AS, et al. Origin and role of a subset of tumor-associated neutrophils with antigen-presenting cell features in early-stage human lung cancer. *Cancer Cell* 2016;**30**:120−35.
34. Jackstadt R, van Hooff SR, Leach JD, Cortes-Lavaud X, Lohuis JO, Ridgway RA, et al. Epithelial NOTCH signaling rewires the tumor microenvironment of colorectal cancer to drive poor-prognosis subtypes and metastasis. *Cancer Cell* 2019;**36**:319−336.e7.
35. He G, Zhang H, Zhou J, Wang B, Chen Y, Kong Y, et al. Peritumoural neutrophils negatively regulate adaptive immunity *via* the PD-L1/PD-1 signalling pathway in hepatocellular carcinoma. *J Exp Clin Cancer Res* 2015;**34**:141.
36. Cristinziano L, Modestino L, Loffredo S, Varricchi G, Braile M, Ferrara AL, et al. Anaplastic thyroid cancer cells induce the release of mitochondrial extracellular DNA traps by viable neutrophils. *J Immunol* 2020;**204**:1362−72.